I&EC research
Industrial & Engineering Chemistry Research

Article

pubs.acs.org/IECR

Scalable Synthesis of Alkali Sulfide Nanocrystals Using a Bubble Column Reactor

Kristen Hietala,[†] Yangzhi Zhao,[‡] Yongan Yang,[‡,§] and Colin A. Wolden*[,†,‡]

[†]Department of Chemical and Biological Engineering, [‡]Materials Science Program, and [§]Department of Chemistry, Colorado School of Mines, 1500 Illinois Street, Golden, Colorado 80401, United States

ABSTRACT: Alkali sulfide nanocrystals (Li_2S and Na_2S) are critical materials used to make solid-state electrolytes and cathodes for advanced battery technologies. We have recently developed a green chemistry for the synthesis of these materials through reactive precipitation by contacting organic solutions with hydrogen sulfide at ambient temperature. In this work, the use of bubble columns was developed as a platform for scalable manufacturing of these nanomaterials. Initial attempts to reproduce the batch reactor synthesis were complicated by nanoparticles clogging the sparger. This was resolved through the introduction of an inert column of fluid between the sparger and the solution. Using this 4-phase bubble column, anhydrous, phase-pure Li_2S and Na_2S nanocrystals were synthesized across the full range of conditions explored. X-ray characterization showed that the primary crystallite size was 20−40 nm, assembling into aggregates of hundreds of nanometers in size. This work validates the potential of bubble columns for large-scale manufacturing of nanocrystals by reactive precipitation in gas−liquid systems.

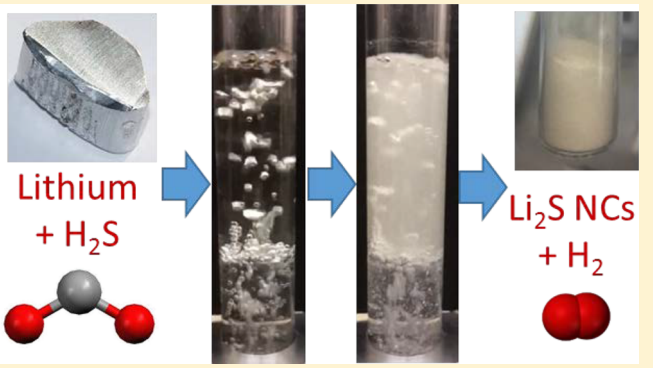

1. INTRODUCTION

The high specific surface area of nanocrystals (NCs) has been demonstrated to be advantageous to numerous technologies, including lubricants,[1] catalysts,[2] sensors,[3] and batteries.[4] The materials of interest in this work are alkali metal sulfides (M_2S, M = Li, Na), which are of great interest for use as cathodes[5,6] or to form solid-state electrolytes[7,8] for use in next generation batteries. Li_2S is of interest for high performance applications[5,7] while the low cost and abundance of sodium makes Na_2S a candidate for stationary storage.[6,8] In battery electrode applications, the high surface area/volume ratio of NCs facilitates efficient insertion/extraction of lithium ions. Cathodes fabricated using NCs demonstrate higher cycling stability, specific capacity, and rate capability relative to bulk materials.[5,9] Nanostructure is also critical for advanced solid-state electrolytes, which are produced by sintering Li_2S with other constituents to make sulfide glasses. It has been shown that reducing the particle size of Li_2S increases the reversible capacity of solid-state cells through improvements in electrolyte conductivity and a reduction of resistance at the electrolyte−electrode interface.[10,11] At present, anhydrous Li_2S and Na_2S materials are only available commercially as micropowders, produced through high temperature carbothermal reduction processes. To create nanoparticles, time- and energy-intensive ball milling processes are typically used, which provide limited control over the final size or morphology.[12,13] Sodium sulfide is a commodity chemical produced through aqueous precipitation and used extensively in pulp and paper production. However, this technique produces the hydrate form $Na_2S{\cdot}xH_2O$ that contains ∼35% water, which is unsuitable for battery applications.

There has been a significant expansion in the number of methods available for environmentally benign synthesis of nanostructures over the past decade.[14] Vapor-phase approaches can offer unique capabilities[15] but are almost always inferior to solution-based techniques from an economic perspective.[16] Reactive precipitation of metal sulfides has long been used to purify hydrometallurgical effluents. In these systems, ammonium sulfate is commonly added to aqueous solutions to induce the precipitation of species such as NiS, ZnS, and CuS.[17] For battery applications, anhydrous metal sulfides are required, precluding the use of aqueous solutions. A common route for the synthesis of metal sulfide NCs is the hot injection method using organic solvents,[18] which produces high quality crystals but faces challenges with respect to scale up.[19]

Our group has recently developed green chemistries for the direct synthesis of M_2S NPs through reactive precipitation by bubbling H_2S through organic solutions containing metal−organic compounds.[20−22] One chemistry for this process employs metal alkoxides as the precursor, which are produced by the dissolution of the alkali metal in alcohol and concomitant release of hydrogen:

Received: April 12, 2018
Revised: June 4, 2018
Accepted: June 6, 2018
Published: June 6, 2018

DOI: 10.1021/acs.iecr.8b01600
Ind. Eng. Chem. Res. XXXX, XXX, XXX−XXX

$$2ROH_{(sol)} + 2M_{(s)} \rightarrow 2ROM_{(sol)} + H_{2(g)} \quad (1)$$

Solvent is then added and synthesis of nanoparticles is accomplished by bubbling hydrogen sulfide (H_2S) through the resulting solution:

$$2ROM_{(sol)} + H_2S_{(g)} \rightarrow M_2S_{(s)} + 2ROH_{(sol)} \quad (2)$$

In this reaction, M_2S NCs precipitate in solution and the alkoxide is converted back into its parent alcohol. The net result of these two reactions is the conversion of a hazardous waste into two high value-added products:

$$2M_{(s)} + H_2S_{(g)} \rightarrow M_2S_{(s)} + H_{2(g)} \quad (3)$$

The individual reactions are both thermodynamically favorable, proceeding rapidly to completion at room temperature, resulting in the complete abatement of H_2S, recovery of H_2, and M_2S NCs synthesis with atom economies approaching unity. This reaction strategy was successfully demonstrated for both Li_2S and Na_2S synthesis.[20] Moreover, it was shown that the NC size and morphology may be tuned through appropriate selection of alcohol and solvent combinations, which may be recycled and reused. The use of lithium as a reagent may give one pause, but Li is required in all advanced battery technologies; in addition, its elemental form provides the highest purity and lowest cost. The economic rationale behind this approach is illustrated by contrasting the cost of the product with the reagent. A 100 g Li foil from Sigma-Aldrich currently costs $301 but can yield 303 g of Li_2S worth >$4000. Previously, these reactions have been demonstrated in a small Parr reactor.[20] This work focuses on developing a scalable process for NC manufacturing.

Synthesis of nanoparticles through reactive precipitation typically involves mixing two liquid solutions to create supersaturation, and these systems are often controlled by mixing at the microscale.[23] As such, a number of innovative reactor designs have been used to extend the degree of control over these parameters including T-junctions,[24] confined impinging jets,[25,26] laminar microfluidic devices,[27] and turbulent micromixers.[1] However, these techniques are not easily scaled nor appropriate for the gas−liquid−solid chemistry involved in this work. Batch or continuous stirred tank reactors are often used for the precipitation process but suffer from broad particle size distributions (PSDs) in systems characterized by fast reactions.[24]

Bubble columns are widely used in the chemical process industry as gas−liquid−solid contactors, because of their simple construction and operation.[28] The bubble column can be run in continuous or semibatch mode, scaled to various dimensions and, in its simplest form, does not contain sensitive mechanical devices such as stirrers. A classic example is production of sodium bicarbonate ($NaHCO_3$) by bubbling CO_2 through sodium hydroxide solutions.[29] More pertinent to this work, bubble columns have been used to remove heavy metal ions such as Zn and Cu from wastewater by precipitating CuS and ZnS when contacted with H_2S.[17] Bubble columns have also been used to remove H_2S from waste effluents.[30] Bubble columns allow for systematic variation of mass transfer, which is anticipated to be important for controlling NC size and aggregation. Critical mass transfer parameters including gas holdup and the bubble diameter may be manipulated through both fluid and geometrical properties using well-established correlations.[31,32]

In this work, we demonstrate the use of bubble columns as a platform for scalable production of anhydrous alkali sulfide (M_2S) nanocrystals. First, the fabrication and characterization of the bubble column is described. Next, its use for synthesis of M_2S NCs is described. It was found that the resulting NCs can clog the pores of the sparger, creating operational problems and compromising the product purity. This challenge was successfully overcome by using fluorinated pump oil as an inert column of fluid between the sparger and the reactive solution. Using this innovative 4-phase bubble column, phase-pure, anhydrous nanocrystals of both Li_2S and Na_2S were successfully produced.

2. METHODS AND MATERIALS

2.1. Reagents. Sodium (Na, ACS reagent, stick dry), ethanol (EtOH, CH_3CH_2OH, anhydrous, containing 0.25% isopropyl alcohol and 0.25% methyl alcohol), the solvent dimethoxyethane (DME, $CH_3OCH_2CH_2OCH_3$, anhydrous, 99.3%), and the solvent dibutyl ether (DBE, $(CH_3(CH_2)_3)_2O$, anhydrous, 99.3%) were purchased from Sigma-Aldrich. Lithium foil (Li, 99.9% trace metals basis, 0.75 mm thick × 19 mm wide) was purchased from Alfa Aesar. Solution preparation and washing/recovery of the resulting NPs were conducted in an Ar-filled glovebox (MBraun LABstar MB10 compact). Fluorinated pump oil (Fomblin Y LVAC 14/6, Specialty Fluids) was used to separate the sparger from solution. Gases employed included a specialty mixture of 10% of H_2S in Ar (Scott Specialty Gases) as well as UHP grade argon.

2.2. Experimental Setup. A schematic of the apparatus used for this work is shown in Figure 1. The column design

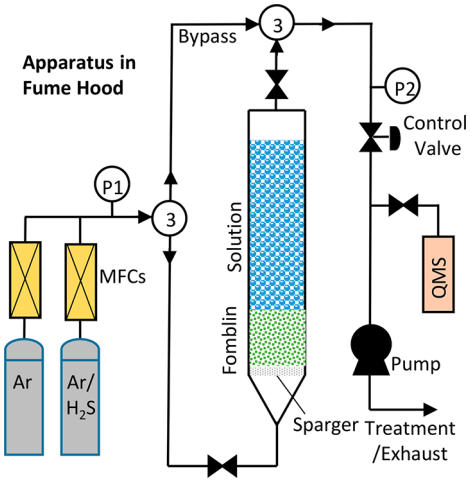

Figure 1. Schematic of the experimental apparatus.

was adapted from the work of Kazakis et al.,[31] who studied bubble formation on porous metal spargers. A 1 in. OD glass tube that was 12 in. in length was secured to the gas handling system with compression seals that were adapted to a 1/4 in. stainless steel tube and terminated with on/off valves. The sparger consisted of a 1/8 in. thick sintered stainless steel disc (McMaster-Carr) that was sealed at the base of the glass tube. Spargers with nominal pore sizes of 2, 10, and 40 μm were employed. Gases were delivered through electronic mass flow controllers and mixed, and a pair of 3-way valves was used to direct the gas mixture either through the bubble column or through a bypass. A needle valve was used to control the

DOI: 10.1021/acs.iecr.8b01600
Ind. Eng. Chem. Res. XXXX, XXX, XXX−XXX

reactor pressure, which was adjusted to operate the reactor just below atmospheric pressure ($P_2 \sim -30$ Torr gauge). The effluent was evacuated using a vacuum pump, and the composition was measured in line using a differentially pumped quadrupole mass spectrometer (QMS, Stanford Research Systems RGA300).

2.3. M_2S NP Synthesis. The metal alkoxide reagent was prepared in the glovebox by first dissolving the alkali metal in EtOH using a 1:8 molar ratio. An appropriate amount of solvent (DME, DBE) was added to make a 0.05 M metal alkoxide (ROM) solution. Approximately 50 mL of solution was transferred to the bubble column and sealed. When employed, an additional 10 mL of Fomblin was added to the column. The column was then transferred to a fume hood and connected to the gas delivery/handling system. Before gas introduction, the gas lines were evacuated to the base pressure of the mechanical pump (<30 mTorr) and the leak rate was tested to ensure the vacuum integrity of the system. During a synthesis experiment, the desired flow/pressure conditions were first established by flowing just Ar. To start an experiment, 40 sccm of the H_2S/Ar mixture was initiated and the diluent Ar flow rate was simultaneously reduced by 40 sccm to ensure minimal disruption to the flow dynamics. H_2S was delivered to the reactor for the amount of time required to make the total molar ratio of ROM to H_2S fixed at the stoichiometric 2:1 ratio (M/S). At this time, the H_2S flow rate was turned off and UHP Ar continued to flow for a couple of minutes, at which time the reactor inlet and outlet valves were closed simultaneously. With the valves closed and sealed, the bubble column was transferred into the Ar-filled glovebox. The column was inverted and allowed to phase separate. The Fomblin was removed first using a separatory funnel and saved for reuse. The reaction solution was centrifuged (15 min, 3100 rpm) to separate the liquid phase and the solid phase. The solid phase was washed several times with solvent from the respective reaction and dried on a hot plate at 80 °C overnight in the glovebox.

2.4. Product Characterization. X-ray diffraction (XRD) patterns were collected on a Philips X'Pert X-ray diffractometer using Cu Kα radiation (λ = 0.15405 nm). The samples were prepared in the Ar-filled glovebox by spreading sample powders onto glass substrates. A drop of mineral oil was used to cover the sample to prevent detrimental reactions with moisture in air when the samples are removed from the glovebox to conduct XRD measurements. The background contributed from the mineral oil (a smooth and broad peak centered at 17.2° spanning from 10° to 25°) was subtracted. Field emission scanning electron microscopy (FE-SEM) images were collected on JEOL JSM-7000F FESEM. FE-SEM samples were prepared by immobilizing the synthesized solid product on a silicon wafer substrate which connects onto an aluminum stub using a double-sided carbon tape.

3. RESULTS AND DISCUSSION

3.1. Bubble Column Characterization. Flow regime is critical to operation and performance of bubble columns. The homogeneous, or bubbly flow regime, is characterized by relatively uniform bubbles well dispersed throughout the column, and this condition is generally observed at superficial velocities $U < 5$ cm/s.[28] In this work, $U < 1$ cm/s and the aspect ratio H/D was between 5 and 10 to ensure good mixing.[28] A key parameter governing mass transport in bubble columns is the specific interfacial area, A, and this quantity is well estimated for spherical bubbles using[33]

$$A = \frac{6\varepsilon_G}{d_B} \quad (4)$$

where ε_G is the gas holdup and d_B is the mean bubble diameter. To assess these parameters, the bubble column dynamics were evaluated by flowing Ar through ethanol/solvent mixtures at atmospheric pressure at total flow rates ranging from 40 to 200 sccm. Photographs of the bubble column as a function of sparger pore size and gas flow rate are summarized in Figure 2.

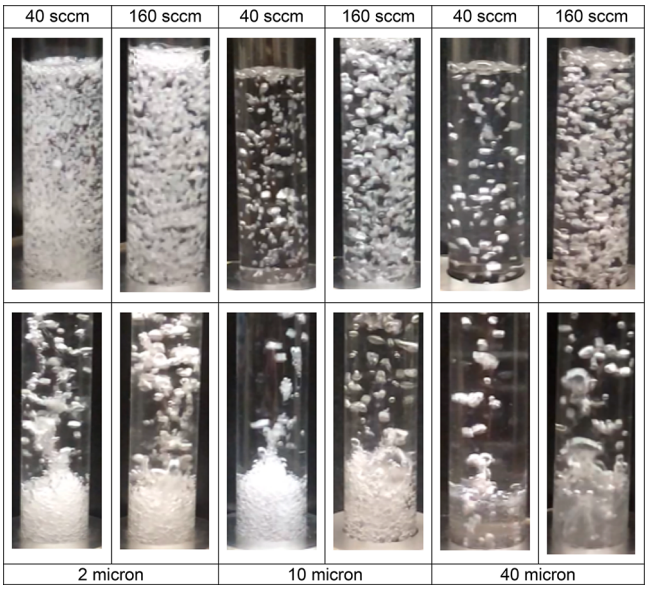

Figure 2. Photographs of the bubble column (OD = 25 mm) as a function of flow rate and sparger pore size without (top row) and with (bottom panel) Fomblin present.

In the absence of Fomblin (top row), the photographs confirm that the column was operated in the homogeneous flow regime. The gas holdup is simply the fraction of the column occupied by gas, and this quantity was determined by measuring the column height with and without gas flow. Figure 3a displays the measured holdup as a function of superficial velocity for different spargers. It is observed that gas holdup increases linearly with superficial velocity, consistent with literature for the bubbly flow regime.[28,34] The pore size of the sparger had a minor impact, with slightly higher holdup values observed with increased pore size.

Bubble size is a complex function of both fluid and geometrical properties that has been well correlated for porous spargers using the following equation[31]

$$\frac{d_B}{d_s} = 7.35\left[We^{-1.7}Re^{0.1}Fr^{1.8}\left(\frac{d_p}{d_s}\right)\right]^{1/5} \quad (5)$$

where d_s and d_p are the sparger diameter and pore size, respectively. The key dimensionless groups include the Weber (We), Reynolds (Re), and Froude (Fr) numbers defined as

$$We = \frac{\rho U^2 d_s}{\sigma} \quad (6)$$

DOI: 10.1021/acs.iecr.8b01600
Ind. Eng. Chem. Res. XXXX, XXX, XXX−XXX

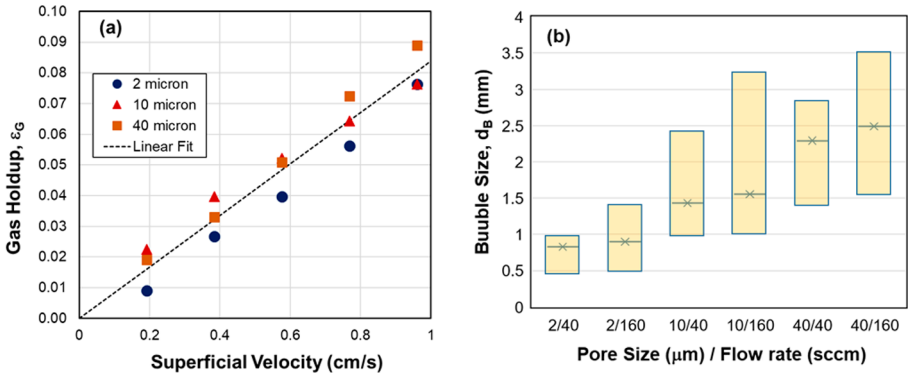

Figure 3. (a) Gas holdup (ε_G) as a function of superficial velocity (U) for spargers with varying pore size. Line is a linear fit to their average values. (b) Comparison of bubble diameter predicted by eq 5 (cross) and experimentally observed range (boxes) for the pore size/flow rate combinations displayed in Figure 2.

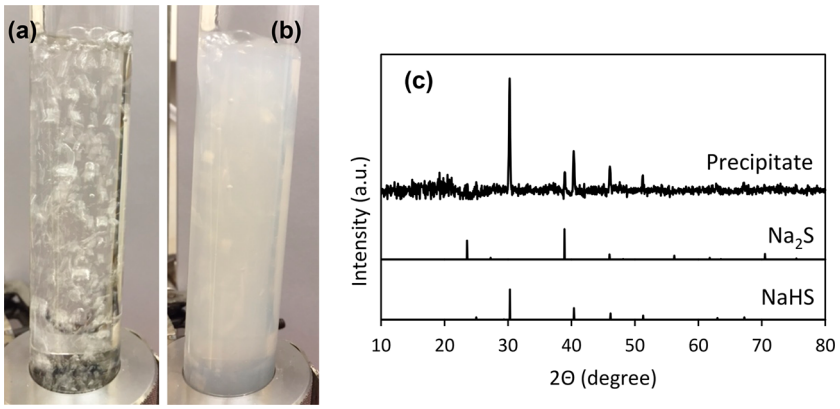

Figure 4. Photographs of the bubble column (a) before introduction of H_2S and (b) near the completion of the run and (c) XRD pattern of the resulting NPs. Conditions: sparger = 10 μm; total flow rate = 80 sccm.

$$Re = \frac{\rho U d_s}{\mu} \tag{7}$$

$$Fr = \frac{U^2}{d_s g} \tag{8}$$

where U is the superficial velocity and ρ, μ, and σ are the density, viscosity, and surface tension of the liquid phase. The photographs in Figure 2 were digitized and analyzed using ImageJ. Figure 3b compares the predictions of eq 5 with the range observed experimentally (boxes). In contrast to gas holdup, bubble size is controlled primarily by the pore size and is relatively insensitive to the superficial velocity. Experimentally, the bubble size distribution is observed to broaden with flow rate, but there is good qualitative agreement with the correlation.

The addition of an ~2.5 cm column of Fomblin dramatically altered the bubble column characteristics (Figure 2). Bubbly flow was maintained within the Fomblin phase, and the bubble size was reduced as expected on the basis of its unique physical properties (SG = 1.9, μ ~ 280 cP). Equation 5 suggests that the bubble diameter in Fomblin should be ~70% of the value in DME/DBE solvents. Despite low superficial velocities, significant bubble coalescence is observed upon the transition from Fomblin into the solvent phase which leads to a much broader bubble size distribution. In the terminology of Bouaifi et al.,[35] this flow regime would be described most accurately as "bad bubbly", in contrast with "perfect bubbly" behavior observed without Fomblin present. When bubbles are formed exiting the sparger, the critical dimension is the pore size as discussed above. During the transition from Fomblin to solvent, the critical dimension is the bubble diameter in the Fomblin phase, which is consistent with the significantly larger bubble sizes observed in the solvent phase at equivalent flow rates. As discussed below, the use of Fomblin was required to prevent clogging of the sparger. Unfortunately, the systematic control over mass transfer demonstrated without Fomblin is lost and the ability to vary mass transfer is limited.

3.2. Nanoparticle Synthesis without Fomblin. Figure 4 displays photographs of the bubble column during the synthesis of sodium sulfide NC and an XRD pattern from the resulting nanomaterials. Before H_2S introduction, the solution is transparent, and the first photograph introduction shows the original bubble size distribution in this experiment. Over the course of the 10 min experiment, the solution becomes increasingly turbid as the NCs precipitate out of solution. Though difficult to see clearly, the bubble dynamics do not appear to be substantially changed by the presence of the NCs. Unfortunately, the material produced was not pure Na_2S but a mixture of materials that was dominated by the NaHS phase. In addition, operational challenges were encountered. The downstream pressure (P_2) remained nominally unchanged, meaning that the flow was continuous throughout the experiment. However, as the experiment proceeded, the upstream pressure (P_1) steadily increased, which was attributed to the NCs clogging the pores and

DOI: 10.1021/acs.iecr.8b01600
Ind. Eng. Chem. Res. XXXX, XXX, XXX−XXX

increasing the pressure drop across the sparger. This suspicion was confirmed by inspection after the reaction where the sparger plate was observed to be clogged with yellow solid. This perhaps was not surprising as the reaction is nearly instantaneous and the Na_2S NCs also have a propensity to settle as their density (SG = 1.86) is much greater than the DME solvent (SG = 0.87).

The clogging of the sparger provides an explanation for the predominance of the NaHS phase. In our previous experience using a small Parr reactor, phase pure Na_2S was obtained as long as the M/H_2S ratio was less than or equal to the stoichiometric value of 2. Once excess H_2S was supplied, NaHS was immediately formed which was attributed to the sequential reaction:[22]

$$Na_2S_{(s)} + H_2S_{(g)} \rightarrow 2NaHS_{(s)} \quad (9)$$

When NCs clog the sparger, they are no longer circulated uniformly throughout the reactor but are exposed to excess H_2S at the inlet, leading to the formation of the NaHS phase.

3.3. M_2S Nanocrystal Synthesis with Fomblin. Several possibilities were considered to overcome the problems encountered with clogging the sparger. One option was to increase the superficial velocity to a sufficient value to prevent this from occurring. However, it was found that this could not be accomplished while maintaining well controlled, homogeneous fluid dynamics within the column. The second thought was to introduce an immiscible column of fluid to separate the sparger from the reactive solution. This intermediate fluid must satisfy a number of requirements. First, it is desirable for the fluid to have a density greater than both the M_2S NCs (SG = 1.66, 1.86) and the organic solvents employed (SG < 1). Second, the fluid needs to be chemically inert with respect to both H_2S and the organic solutions employed. Good thermal stability and low volatility would also be beneficial. A fluid that was found to satisfy all these requirements was fluorinated pump oil, sold commercially under the trade name Fomblin. Commonly used to pump corrosive and reactive gases, this fluid behaves essentially like liquid Teflon: it is dense (SG ~ 1.9), possesses low volatility ($<10^{-7}$ Torr), is chemically inert, and is completely immiscible with the solutions employed.

Fomblin was added to the column, where it naturally settled to the base, and the resulting 4-phase bubble column (2 fluids + gas + solid) was evaluated for the production of anhydrous M_2S nanocrystals. Figure 5 displays photographs of the bubble column in operation during nanocrystal synthesis. The immiscible nature of the two fluids is confirmed by the distinct interface shown in each picture. The first photograph displays the bubble distribution at the start of the experiment. As expected from physical properties, the bubbles are much smaller in the Fomblin phase. They coalesce into larger bubbles at the interface but generally remain spherical and isolated as they ascend through the solution. The bubble dynamics remain substantially unchanged upon H_2S introduction and NC precipitation. In-line QMS monitoring of the effluent confirmed complete H_2S abatement throughout these experiments. H_2S is about 20× more soluble in organic solutions than water,[36] so issues related to limited absorption observed in aqueous systems are not encountered here.[30] The effectiveness of Fomblin at separating NCs is shown by the fact that this phase remains clear even late into the reaction. Moreover, no change in pressure drop was observed throughout the course of these experiments, and postreaction inspection found no solids on the sparger. The last photograph

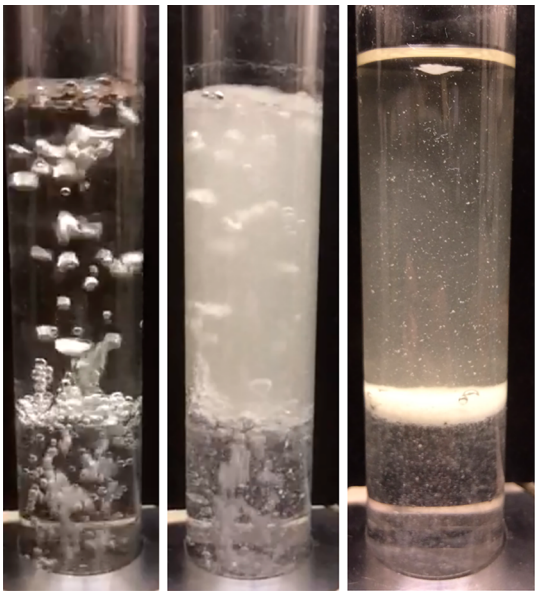

Figure 5. Photographs of the 4-phase bubble column during NC synthesis. From left to right: near the start of the reaction, near completion, and after the reaction was complete and the gas flow was stopped. Reaction conditions were with NaOEt/DBE with 40 sccm of H_2S/Ar mix and 40 sccm diluent Ar.

was taken a few minutes after the gas flow was turned off. The NCs rapidly settle out of the solution, forming a dense layer at the interface. After settling, a separatory funnel was used to separate and dispense the individual phases (Fomblin, NCs, and solution).

The NCs were rinsed with solvent and dried, and Figure 6 displays XRD patterns obtained from the NCs produced in the 4-phase column. Anhydrous, phase-pure Na_2S and Li_2S NCs were synthesized across the full range of flow rates examined. No evidence of the NaHS phase or any other impurities are observed. In addition, no deposition was observed on the sparger. The flow rate did not appear to have a significant impact on the properties of the NCs over the range examined. A Scherrer analysis was used to estimate the size of the resulting NCs, which was found to be 37 ± 5 and 23 ± 5 nm for Na_2S and Li_2S, respectively. The yield of NCs relative to the amount expected on the basis of the mass of alkali metal dissolved was consistently around 87%. Both Li_2S and Na_2S have some solubility in ethanol,[37] which is generated as the reaction proceeds, and this accounts for the majority of the material that is lost. Additional amounts are lost through handling process. It should be noted that the solution may be recycled and reused as demonstrated previously,[20] enabling recovery of soluble M_2S.

Finally, the morphology of the NCs was evaluated using FE-SEM imaging as shown in Figure 7, which compares NCs obtained in a batch reactor with those obtained using the bubble column. For both materials, the primary NCs aggregate into larger particles. In the case of Na_2S, the aggregates formed in the bubble column (200−500 nm) are significantly larger than those in the batch reactor (~50 nm). In contrast, the Li_2S NCs produced in the bubble column appear smaller and more homogeneous than what was produced in the batch reactor. The Li_2S NCs have the form of flakes or platelets that assemble into porous aggregates. For both materials, the bubble column produced highly uniform particles. As demonstrated pre-

DOI: 10.1021/acs.iecr.8b01600
Ind. Eng. Chem. Res. XXXX, XXX, XXX−XXX

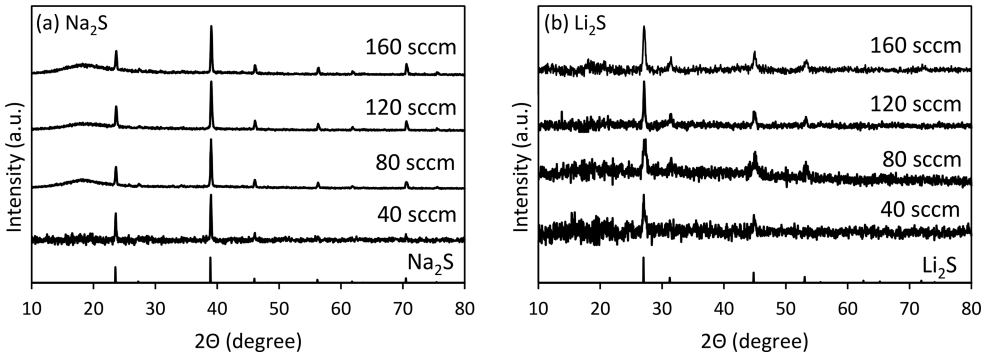

Figure 6. XRD patterns of the (a) Na_2S and (b) Li_2S NCs produced in the 4-phase bubble column.

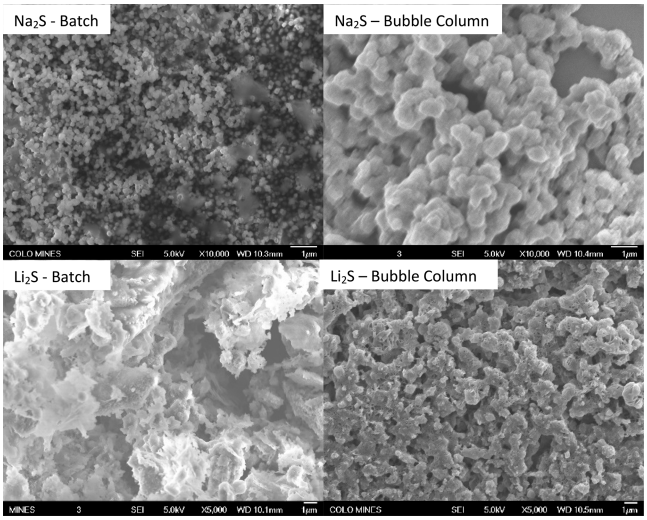

Figure 7. Comparison of FE-SEM images of Na_2S (top) and Li_2S (bottom) NCs synthesized in a batch reactor (left) and the 4-phase bubble column (right).

viously, the size and morphology of the M_2S NCs can be tuned by choice of solvent, alcohol, and composition. Having established a robust platform for NC synthesis, work is underway to further refine the materials produced using this technique and evaluate their electrochemical performance.

4. CONCLUSIONS

In this work, we have demonstrated the potential of bubble columns for the production of alkali sulfide nanocrystals through reactive precipitation. One challenge caused by the fast reaction kinetics and the large density of the M_2S was blockage of the sparger by the NCs, creating operational problems and producing undesired phases such as NaHS. This challenge was overcome by the insertion of a column of Fomblin pump oil to separate the reactive solution from the sparger. The use of the secondary fluid attenuates the degree of control over bubble size but results in the production anhydrous, phase-pure Li_2S and Na_2S nanocrystals across the range of conditions explored. X-ray characterization showed that the primary particle size was 20−40 nm, assembling into submicron aggregates. This work validates the promise of bubble columns for large scale manufacturing of nanocrystals by reactive precipitation in gas−liquid systems. The 4-phase bubble column provides an innovative platform for reactive precipitation processes where blockage of the sparger is a potential concern.

AUTHOR INFORMATION

Corresponding Author

*E-mail: cwolden@mines.edu.

ORCID

Yongan Yang: 0000-0003-1451-2923

Colin A. Wolden: 0000-0001-6576-048X

Notes

The authors declare no competing financial interest.

ACKNOWLEDGMENTS

This work is financially supported by the Colorado Office of Economic Development and International Trade (COEDIT). K.H. gratefully acknowledges the support of a Mines Undergraduate Research Fellowship.

REFERENCES

(1) Santillo, G.; Deorsola, F. A.; Bensaid, S.; Russo, N.; Fino, D. MoS_2 nanoparticle precipitation in turbulent micromixers. *Chem. Eng. J.* **2012**, *207-208*, 322−328.

(2) Jaramillo, T. F.; Jorgensen, K. P.; Bonde, J.; Nielsen, J. H.; Horch, S.; Chorkendorff, I. Identification of active edge sites for electrochemical H_2 evolution from MoS_2 nanocatalysts. *Science* **2007**, *317* (5834), 100−102.

(3) Lee, H.; Yoon, S. W.; Kim, E. J.; Park, J. In-situ growth of copper sulfide nanocrystals on multiwalled carbon nanotubes and their application as novel solar cell and amperometric glucose sensor materials. *Nano Lett.* **2007**, *7* (3), 778−784.

(4) Robinson, J. P.; Koenig, G. M. Tuning solution chemistry for morphology control of lithium-ion battery precursor particles. *Powder Technol.* **2015**, *284*, 225−230.

(5) Wu, F.; Lee, J. T.; Fan, F.; Nitta, N.; Kim, H.; Zhu, T.; Yushin, G. A hierarchical particle-shell architecture for long-term cycle stability of Li_2S cathodes. *Adv. Mater.* **2015**, *27* (37), 5579−5586.

(6) Wei, S.; Xu, S.; Agrawral, A.; Choudhury, S.; Lu, Y.; Tu, Z.; Ma, L.; Archer, L. A. A stable room-temperature sodium-sulfur battery. *Nat. Commun.* **2016**, *7*, 11722.

(7) Kato, Y.; Hori, S.; Saito, T.; Suzuki, K.; Hirayama, M.; Mitsui, A.; Yonemura, M.; Iba, H.; Kanno, R. High-power all-solid-state batteries using sulfide superionic conductors. *Nature Energy* **2016**, *1*, 16030.

(8) Hayashi, A.; Noi, K.; Sakuda, A.; Tatsumisago, M. Superionic glass-ceramic electrolytes for room-temperature rechargeable sodium batteries. *Nat. Commun.* **2012**, *3*, 856.

(9) Yang, Y.; McDowell, M. T.; Jackson, A.; Cha, J. J.; Hong, S. S.; Cui, Y. New nanostructured Li_2S/Silicon rechargeable battery with high specific energy. *Nano Lett.* **2010**, *10* (4), 1486−1491.

(10) Zhang, Y.; Chen, R.; Liu, T.; Shen, Y.; Lin, Y.; Nan, C.-W. High capacity, superior cyclic performances in all-solid-state lithium-ion batteries based on $78Li_2S$-$22P_2S_5$ glass-ceramic electrolytes prepared via simple heat treatment. *ACS Appl. Mater. Interfaces* **2017**, *9* (34), 28542−28548.

DOI: 10.1021/acs.iecr.8b01600
Ind. Eng. Chem. Res. XXXX, XXX, XXX−XXX

(11) Yu, C.; Ganapathy, S.; Eck, E. R. H. v.; Wang, H.; Basak, S.; Li, Z.; Wagemaker, M. Accessing the bottleneck in all-solid state batteries, lithium-ion transport over the solid-electrolyte-electrode interface. *Nat. Commun.* **2017**, *8* (1), 1086.
(12) Rabanal, M. E.; Gutierrez, M. C.; Garcia-Alvarado, F.; Gonzalo, E. C.; Arroyo-de Dompablo, M. E. Improved electrode characteristics of olivine−$LiCoPO_4$ processed by high energy milling. *J. Power Sources* **2006**, *160* (1), 523−528.
(13) Cai, K.; Song, M.-K. K.; Cairns, E. J.; Zhang, Y. Nanostructured Li_2S-C composites as cathode material for high-energy lithium/sulfur batteries. *Nano Lett.* **2012**, *12* (12), 6474−6479.
(14) Patete, J. M.; Peng, X. H.; Koenigsmann, C.; Xu, Y.; Karn, B.; Wong, S. S. Viable methodologies for the synthesis of high-quality nanostructures. *Green Chem.* **2011**, *13* (3), 482−519.
(15) Thimsen, E.; Kortshagen, U. R.; Aydil, E. S. Nonthermal plasma synthesis of metal sulfide nanocrystals from metalorganic vapor and elemental sulfur. *J. Phys. D: Appl. Phys.* **2015**, *48* (31), 314004.
(16) Osterwalder, N.; Capello, C.; Hungerbuhler, K.; Stark, W. J. Energy consumption during nanoparticle production: How economic is dry synthesis? *J. Nanopart. Res.* **2006**, *8* (1), 1−9.
(17) Al-Tarazi, M.; Heesink, A. B. M.; Versteeg, G. F.; Azzam, M. O. J.; Azzam, K. Precipitation of CuS and ZnS in a bubble column reactor. *AIChE J.* **2005**, *51* (1), 235−246.
(18) Joo, J.; Na, H. B.; Yu, T.; Yu, J. H.; Kim, Y. W.; Wu, F.; Zhang, J. Z.; Hyeon, T. Generalized and facile synthesis of semiconducting metal sulfide nanocrystals. *J. Am. Chem. Soc.* **2003**, *125* (36), 11100−11105.
(19) Pu, Y.; Cai, F.; Wang, D.; Wang, J.-X.; Chen, J.-F. Colloidal synthesis of semiconductor quantum dots toward large-ccale production: A Review. *Ind. Eng. Chem. Res.* **2018**, *57* (6), 1790−1802.
(20) Li, X.; Zhao, Y.; Brennan, A.; McCeig, M.; Wolden, C. A.; Yang, Y. Reactive precipitation of anhydrous alkali sulfide nanocrystals with concomitant abatement of hydrogen sulfide and cogeneration of hydrogen. *ChemSusChem* **2017**, *10*, 2904−2913.
(21) Li, X.; Wolden, C. A.; Ban, C.; Yang, Y. Facile synthesis of lithium sulfide nanocrystals for use in advanced rechargeable batteries. *ACS Appl. Mater. Interfaces* **2015**, *7* (51), 28444−28451.
(22) Li, X.; Morrish, R. M.; Yang, Y.; Wolden, C. A.; Yang, Y. Thermodynamically favorable conversion of hydrogen sulfide into valuable products through reaction with sodium naphthalenide. *ChemPlusChem* **2015**, *80* (10), 1508−1512.
(23) Wang, L. G.; Fox, R. O. Comparison of micromixing models for CFD simulation of nanoparticle formation. *AIChE J.* **2004**, *50* (9), 2217−2232.
(24) Kawase, M.; Miura, K. Fine particle synthesis by continuous precipitation using a tubular reactor. *Adv. Powder Technol.* **2007**, *18* (6), 725−738.
(25) Liu, Y.; Fox, R. O. CFD predictions for chemical processing in a confined impinging-jets reactor. *AIChE J.* **2006**, *52* (2), 731−744.
(26) Marchisio, D. L.; Rivautella, L.; Barresi, A. A. Design and scale-up of chemical reactors for nanoparticle precipitation. *AIChE J.* **2006**, *52* (5), 1877−1887.
(27) Li, S. W.; Xu, H. H.; Wang, Y. J.; Luo, G. S. Controllable preparation of nanoparticles by drops and plugs flow in a microchannel device. *Langmuir* **2008**, *24* (8), 4194−4199.
(28) Shah, Y. T.; Kelkar, B. G.; Godbole, S. P.; Deckwer, W. D. Design parameters estimations for bubble column reactors. *AIChE J.* **1982**, *28* (3), 353−379.
(29) Goharrizi, A. S.; Abolpour, B. Estimation of sodium bicarbonate crystal size distributions in a steady-state bubble column reactor. *Res. Chem. Intermed.* **2012**, *38* (7), 1389−1401.
(30) Esmaeili-Faraj, S. H.; Nasr Esfahany, M. Absorption of hydrogen sulfide and carbon dioxide in water based nanofluids. *Ind. Eng. Chem. Res.* **2016**, *55* (16), 4682−4690.
(31) Kazakis, N. A.; Mouza, A. A.; Paras, S. V. Experimental study of bubble formation at metal porous spargers: Effect of liquid properties and sparger characteristics on the initial bubble size distribution. *Chem. Eng. J.* **2008**, *137* (2), 265−281.
(32) öztürk, S. S.; Schumpe, A.; Deckwer, W. D. Organic liquids in a bubble column: Holdups and mass transfer coefficients. *AIChE J.* **1987**, *33* (9), 1473−1480.
(33) Euzen, J.-P.; Trambouze, P. *Chemical Reactors: From Design to Operation*; Editions Technip: Paris, 2004.
(34) Kawagoe, K.; Inoue, T.; Nakao, K.; Otake, T. Flow pattern gas hold-up conditions in gas sparged contactors. *Int. Chem. Eng.* **1976**, *16*, 176−184.
(35) Bouaifi, M.; Hébrard, G.; Bastoul, D.; Roustan, M. A comparative study of gas hold-up, bubble size, interfacial area and mass transfer coefficients in stirred gas−liquid reactors and bubble columns. *Chem. Eng. Process.* **2001**, *40*, 97−111.
(36) Bryk, S. D.; Makitra, R. G.; Pal'chikova, E. Y. Solubility of hydrogen sulfide in organic solvents. *Russ. J. Inorg. Chem.* **2006**, *51* (3), 506−511.
(37) Kurzin, A. V.; Evdokimov, A. N.; Golikova, V. S.; Pavlova, O. S. Solubility of sodium sulfide in alcohols. *J. Chem. Eng. Data* **2010**, *55* (9), 4080−4081.

DOI: 10.1021/acs.iecr.8b01600
Ind. Eng. Chem. Res. XXXX, XXX, XXX−XXX